The phase structure of high-pressure-crystallized polyethylene

R. Kitamaru*, F. Horii and Q. Zhu†
*Institute for Chemical Research, Kyoto University, Uji City, Kyoto 611, Japan and *Science and Technology, Ryukoku University, Seta, Otsu 520, Japan*

and D. C. Bassett‡ and R. H. Olley
J. J. Thomson Physical Laboratory, University of Reading, Reading RG6 2AF, UK
(Received 6 January 1992; revised 8 July 1993)

The phase structure of three linear polyethylene (PE) samples, crystallized from the melt at high pressure, has been studied by electron microscopy and high-resolution solid-state ^{13}C n.m.r. spectroscopy. In general, three phases are required to account for the n.m.r. data: the lamellar crystalline phase, the crystalline–amorphous interphase and the amorphous phase. All three are present in high-molecular-weight samples but there is no amorphous phase for samples with lower molecular weights and large lamellar thicknesses. The amorphous phase appears when the ratio of the number-averaged extended molecular chain length (X_n) to the number-averaged crystalline stem length (L_n) exceeds two. High-pressure-crystallized materials differ from those crystallized at atmospheric pressure in that the mass fraction of the amorphous phase does not exceed 0.05; the thickness of the crystalline–amorphous interphase reaches 8.0 nm for material with the highest molecular weight, a value which is considerably larger than those reported for samples crystallized at atmospheric pressure or which have been estimated theoretically. Extraordinarily long ^{13}C spin-lattice relaxation times have been found: a figure of $T_{1C} = 7000$ s, higher than any previously reported, for the highest-molecular-weight sample is still less than would be expected from the large lamellar thickness. In consequence, this relaxation is attributed to molecular motion in the vicinity of the crystal defects; this is in addition to ^{13}C spin diffusion to the non-crystalline region, occurring with a shorter T_{1C}. The discrepancy between the observed and calculated values of T_{1C} increases as the molecular weight falls in those samples for which the crystal stem lengths exceed the extended molecular lengths. For these, the unexpectedly shorter T_{1C} is attributed to defects such as methyl end-groups within the crystalline regions.

(Keywords: high-pressure crystallization; polyethylene; solid-state n.m.r.)

INTRODUCTION

Polymers are complex materials in which elucidation of the details of their internal organization requires input from a range of complementary techniques. All too often, however, different techniques are applied in isolation to different samples of a polymer which may differ substantially, e.g. in molecular weight and preparative conditions. The aim of this paper is to combine the results obtained from n.m.r. spectroscopy and electron microscopy on the same series of samples of linear polyethylene, in order to obtain a better understanding of their phase structure. The materials chosen have been crystallized at high pressure, which produces samples of the highest crystallinity which are arguably the least complicated of melt-crystallized polyethylenes, so that the prospects of obtaining definitive conclusions are enhanced.

The phase structure of crystalline linear polyethylene differs widely according to its molecular-weight distribution, and the thermal and mechanical history of the sample. Some of the present authors have examined the phase structure of samples crystallized isothermally from the melt or dilute solution under atmospheric pressure, using high-resolution ^{13}C n.m.r. analysis[1]. In melt-crystallized samples they found three distinct phases differing in their ^{13}C chemical shift and relaxation behaviour, namely the lamellar crystalline phase, the noncrystalline amorphous phase which shows rubbery molecular motion, and the crystalline–amorphous interphase which has less molecular motion. The thickness of the crystalline–amorphous interphase is ~ 34 Å for samples with molecular weights of 30 000–150 000. Such a phase structure is thought to differ according to the precise conditions of formation, especially when employing very high pressures to produce crystalline lamellae of an extremely large thickness. These are the phenomena which are explored in this present paper.

EXPERIMENTAL

Samples

Two different molecular-weight fractions with weight-average molecular weights of 28 600 (Fraction 2) and 33 000 (Fraction 1), and three unfractionated whole polymers with weight-average molecular weights of

† Present address: University of Science and Technology of China, Hefei, China
‡ To whom correspondence should be addressed

0032-3861/94/06/1171–11

132 000 (BP Rigidex 9), 231 000 (BP H020-54P) and 1.1×10^6 (Hercules Hifax 1900) were used in this work. They were melted at 260°C for 1 h at 4.95 kbar and then cooled slowly. Cooling rates over the range of crystallization temperatures were 0.25 K min^{-1} for the PE fractions (1 and 2), and 2 K min^{-1} for the Rigidex 9, H020-54P and Hifax materials.

The crystalline fractions of the polymers were determined in a density gradient column, using toluene and carbon tetrachloride at 23°C, and are based on a crystalline density of 1.002 and a noncrystalline density of 0.8531, after Jackson *et al.*[2]. They were also estimated by broad-line proton n.m.r. lineshape analysis[3,4], as well as by ^{13}C n.m.r. lineshape analysis, according to the method described below. Differential scanning calorimetry was carried out using a Perkin–Elmer DSC-2C, at a heating rate of 10 K min^{-1}, with calibration against high-purity indium, taking the peak of the melting endotherm as the melting temperature. All of these values are given in *Table 1*.

Molecular weight distributions

These were obtained by gel permeation chromatography[5] for the original materials, for the samples after high-pressure crystallization, and after nitric acid degradation of the crystallized materials.

Electron microscopy

Two stage replicas, obtained according to standard procedures, were obtained for fracture surfaces prepared under liquid nitrogen, and cut surfaces etched with a 0.7% (wt/vol) solution of $KMnO_4$ in H_2SO_4/H_3PO_4 (2/1) at room temperature[6]. Micrographs of the fracture surfaces were used to measure the distribution of crystal thicknesses.

^1H broad-line n.m.r. spectroscopy

The ^1H broad-line n.m.r. spectra of the pressure-crystallized samples were obtained at room temperature using a field intensity of 1.4 T (60 MHz ^1H Larmor frequency) and decomposed into three components, namely the broad, medium and narrow components, as previously described[3].

^{13}C n.m.r. spectroscopy

Experiments involving dipolar decoupling (DD), and magic angle spinning (MAS), were performed as follows: ^1H DD/MAS ^{13}C n.m.r. measurements were carried out at room temperature using a JEOL JNM-FX200 spectrometer operating at a field strength of 4.7 T. The radio frequency of 50.1 MHz, with a field strength B_1 of 6.6–6.5 mT ($\gamma B_1/2\pi = 64.1$–69.4 kHz), was used for detection of the ^{13}C resonance. The ^1H DD field was 1.4 mT (53.9 kHz). MAS experiments were carried out at a rate of 3.3–3.5 kHz with a cylinder-type rotor made of Al_2O_3 and poly (amide–amide) resins, with a volume of $\sim 0.16\,cm^3$. The chemical shifts relative to tetramethylsilane (TMS) were determined from the CH line (29.50 ppm) of solid adamantane used as an external standard.

RESULTS AND DISCUSSION

General remarks

All samples that were examined exhibited a lamellar crystalline structure, with very large lamellar thicknesses and high degrees of crystallinity (see *Table 1*). The crystallinity is very high for the two low-*MW* fractions and although it decreases with increasing molecular weight it is still as high as 0.83–0.87 for the Hifax sample, which has the highest weight-average molecular weight of 1.1×10^6.

The thicknesses of the crystalline lamellae cover a spectrum of values, but *Table 1* gives the number-average values obtained by using electron microscopy or g.p.c. analysis. For most samples the d.s.c. thermograms exhibited multiple peaks. The highest peak melting temperature, T_m, of each sample is generally above 140°C, as expected for the pressure-crystallized samples with their large lamellar thicknesses. Nevertheless, the reported T_m of 147.2°C for the highest-molecular-weight-sample, namely Hifax 1900, is above the accepted equilibrium melting temperature of this polymer as a result of superheating. As expected, some lowering of T_m (by 1–2 K) was observed when the heating rate was decreased from 10 to 1.25 K min^{-1}. The presence of multiple peaks is a consequence of discrete populations within the wide distribution of crystalline lamellae.

The crystalline stem length as revealed by g.p.c.

G.p.c. curves were obtained for all of the original samples, their pressure-crystallized products, and further

Table 1 Characterization of PE samples

Sample	M_w[a]	M_w/M_n	Degree of crystallinity		Crystal thickness (nm)	T_m[d] (°C)
			Density[b]	^1H n.m.r.[c]		
Fraction 2	28 600	1.22	0.971	0.928	457[e]	140.1
						139.7
Fraction 1	33 000	1.25	0.972	0.944	580[e]	140.0
Rigidex 9	132 000	10.4	0.928	0.898	82[f]	140.3
						132.2
						125.8
HO20-54P	231 000	8.2	0.931	0.878	120[f]	142.3
						125.6
Hifax 1900	1.1×10^6		0.869	0.834	190[f]	147.2

[a] Estimated by g.p.c.
[b] Estimated from density gradient measurements
[c] Obtained by 3-component analyses of broad-line ^1H n.m.r.
[d] Peak temperature found in a d.s.c. thermogram measured at a rate of 10 K min^{-1}
[e] Number-averaged crystal thicknesses determined from electron micrographs
[f] Number-averaged lamellar thicknesses determined by nitration/g.p.c. method

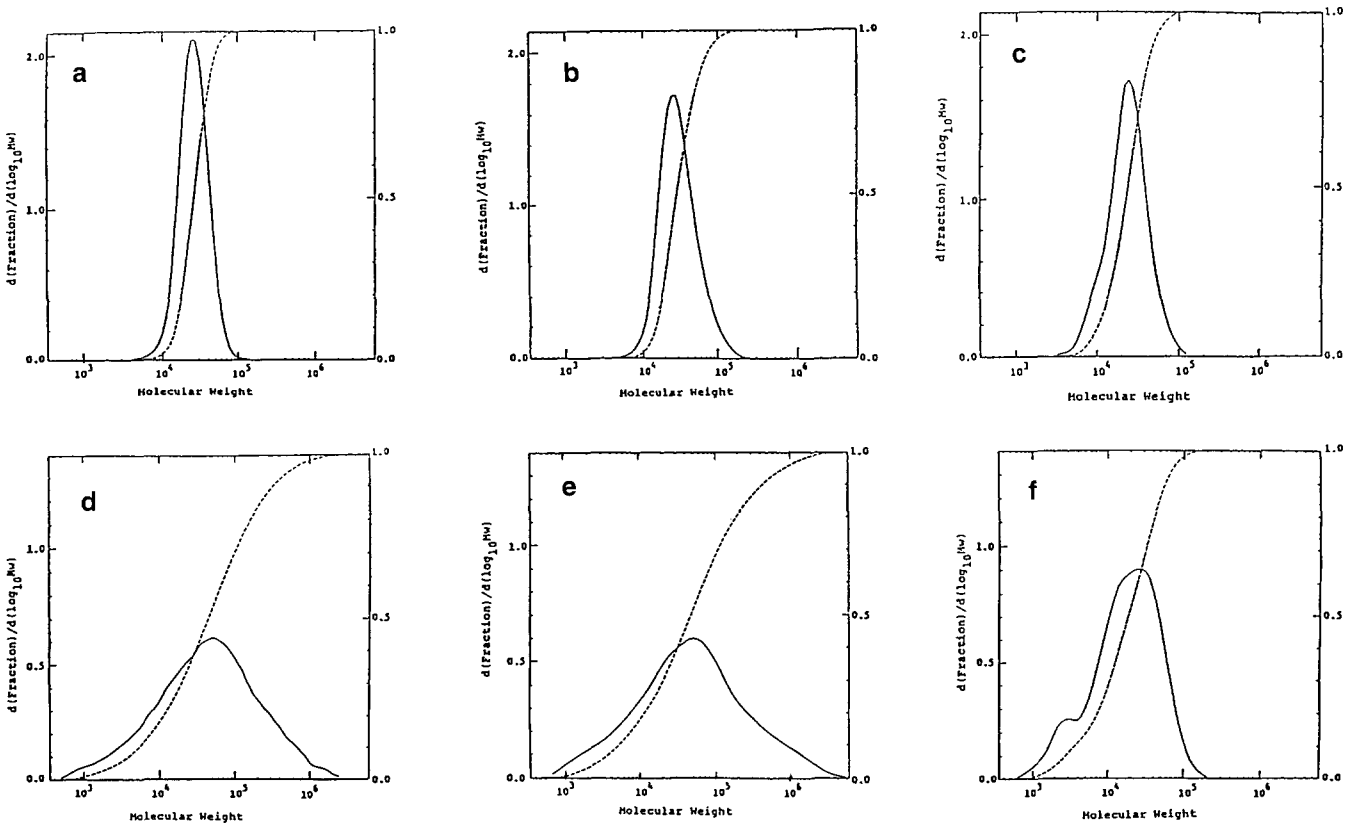

Figure 1 G.p.c. curves (continuous lines) and derived cumulative distributions (broken lines) for different polyethylene samples: (a) Fraction 2; (b) Fraction 2, pressure crystallized; (c) Fraction 2, nitrated; (d) Rigidex 9; (e) Rigidex 9, pressure crystallized and; (f) Rigidex 9, nitrated

Table 2 Number- and weight-average molecular chain lengths obtained from g.p.c. analyses for original, nitrated, and pressed samples[a]

Sample	Number-average molecular chain length, X_n (nm)	Weight-average molecular chain length, X_w (nm)	X_w/X_n
Fraction 2			
Original	210	260	1.22
Pressed	240	330	1.38
Nitrated	180	250	1.40
Fraction 1			
Original	240	300	1.25
Pressed	280	420	1.51
Nitrated	180	270	1.51
Rigidex 9			
Original	110	1 200	10.4
Pressed	120	1 600	13.4
Nitrated	82	240	2.90
H020-54P			
Original	260	2 100	8.2
Nitrated	120	280	2.26
Hifax 1900			
Original	–	10 000	–
Nitrated	190	380	1.99

[a] Pressed = pressure crystallized sample

nitric acid treated products. The results obtained for Fraction 2 and Rigidex 9 are given as examples in *Figure 1*. The number- and weight-average molecular chain lengths, X_n and X_w, respectively, were estimated from these g.p.c. curves and are given in *Table 2*, along with their X_w/X_n values. It has previously been shown that the nitric acid treatment leads to decomposition of the noncrystalline material among the lamellar crystallites, thus retaining only crystalline material[5]. Hence, the g.p.c. curve of the nitric acid treated samples is expected to give the crystalline stem length. It is first noted for Fractions 2 and 1, with the lowest molecular weights, that the number-average molecular chain lengths of 210 and 240 nm, respectively, estimated from g.p.c. are significantly shorter than the corresponding values of 457 and 580 nm obtained by electron microscopy (see *Table 1*). This evidently implies that molecular end groups (CH_3 and $CH{=}CH_2$) are included in the crystalline lamellae[5]. Secondly, it is seen in the cumulative g.p.c. curves (see *Figure 1*) that there is rather more material at the higher-molecular-weight end of the distributions of the high-pressure crystallized products than found in those of the respective original samples. One should note for example, the proportion larger than 10^5 for Fraction 2 (*Figures 1a* and *1b*) and above 10^6 in Rigidex 9 (*Figures 1d* and *1e*). This may imply that some intermolecular crosslinking has begun to occur during the pressure crystallization at 4.95 kbar, as previously reported at 9 kbar[7]. The average molecular chain lengths, X_w or X_n, of the nitrated samples generally indicate the average crystalline stem lengths, but this is not possible for Fractions 1 and 2 because of the incorporation of molecular chain ends in the crystalline region. For these samples, we rely on electron microscopy data for the crystalline stem length[5]. For the whole polymer, Rigidex 9, (*Figure 1f*) there are two peaks in the distribution: the thicker lamellae grow first, while the thinner population contains shorter molecules, as a consequence of fractional crystallization by molecular weight[8,9]. In the g.p.c. curves of the nitrated products of each sample the distribution of the crystalline stem length appears somewhat larger than that expected from the electron microscopy studies.

In fact, when the treatment of Hifax with nitric acid was prolonged for a period of 18 days, the larger-molecular-weight fraction was somewhat decreased, suggesting that some chain folds are located only a few Å below the general fold surface and these had become accessible during this prolonged acid treatment.

Lamellar structure from electron micrographs

Figure 2a shows the electron micrograph of Fraction 2. Lamellae thicker than 3 μm are sometimes seen, e.g. at the upper left of the photograph, but generally there are two groups of lamellae, namely the thicker lamellae of 1–2 μm and the thinner lamellae of $\sim$0.1 μm. In the photograph of *Figure 2b* (Fraction 1), again lamellae thicker than 3 μm are sometimes recognized, but lamellar thicknesses are generally smaller than in Fraction 2. The photograph shown in *Figure 2c* indicates the lamellar structure of Rigidex 9. It is seen that there are few lamellae thicker than 1 μm and that thicknesses of 0.3–0.5 μm are typical. Between these typical lamellae there are many thinner lamellae which are packed parallel. *Figure 2e* shows that the lamellar structure of Hifax consists of two components which differ in the nucleation density, as is seen in the upper and lower parts of the photograph. *Figures 2f* and *2g* are the enlarged photographs of these typical parts, with low and high nucleation, respectively. The thickness of the lamellae in the former part is $\sim$0.3 μm, while in the latter it is $\sim$0.2 μm.

For Fractions 1 and 2 the crystal thicknesses were read off at every part of a lattice superimposed on the photographs. *Figure 3* gives a histogram of the crystal thickness for each of the fractions; the area of each box is proportional to the mass fraction within the given range, and resolution for each measurement is as good as, or better than, the width of the histogram box. Both distributions appear bimodal; while the lower part, however, corresponds in value to the extended molecular chain length, the upper part is considerably greater, indicating incorporation of the chain ends in the crystalline phase[5].

^{1}H broad-line n.m.r. spectroscopy

Line shape analyses of broad-line ^{1}H n.m.r. spectra allows us to explore the phase structure of samples in terms of the difference in overall molecular motion of each phase via the line width determined by the time fluctuation of magnetic dipole–dipole interactions between ^{1}H nuclei of the order of $\sim 10^6$ Hz. In polyethylenes we find components of broad, medium and narrow linewidth: for samples crystallized at amospheric pressure these have previously been assigned, respectively, to the crystalline (broad), rubbery amorphous (medium), and interfacial (narrow) phase[3]. The mass fractions of these components are shown in *Figure 4* as a function of weight-average molecular weight, including an additional PE specimen ($MW = 10^5$) supplied by Professor K. Ito of Kyoto Art and Technology University. Previous data for atmospheric-pressure samples are shown for comparison by the broken line in the figure. In the latter, it is seen that in the molecular weight range lower than 20 000, the samples consist only of crystalline lamellae and a non-crystalline overlayer. Above this, the rubbery amorphous phase with rubbery molecular motion appears and its mass fraction continues to increase with molecular weight; the noncrystalline overlayer also starts to increase above a MW of 20 000. On the other hand, for the high-pressure-crystallized samples, the rubbery amorphous phase does not appear below a MW of 100 000, and is only just discernible in Rigidex 9 with a MW of 132 000 (above the upper solid line, with data shown by open circles). Beyond this molecular weight, the rubbery amorphous phase increases concomitantly with decreasing crystallinity but to lesser extent in comparison with that found in the case of the atmospheric-pressure-crystallized samples; even above a MW of 10^6 its mass fraction hardly exceeds 10%, and the degree of crystallinity remains as high as 80%. This seems to be characteristic of the samples crystallized at high pressure.

High-resolution solid.state ^{13}C n.m.r. spectroscopy

DD/MAS ^{13}C n.m.r. spectra. While ^{1}H broad-line n.m.r. spectroscopy detects the overall molecular motion of each phase, high-resolution solid-state ^{13}C n.m.r. spectroscopy can detect the chemical shift of each component carbon by eliminating the effect of the dipole–dipole interaction. Since the chemical shift is determined by detailed molecular conformation, ^{13}C n.m.r. spectroscopy can (by means of differences of chemical shift and the longitudinal and transverse relaxations) provide more detailed information about the actual structure of each phase in terms of the molecular chain conformation and the chain motion over a wide range of frequencies. In particular, it can distinguish more clearly between the rubbery amorphous and the interphase materials. Both phases are associated with an equivalent spin-lattice relaxation time T_{1C} of 0.5 s, but while the former is associated with a spin–spin relaxation time, T_{2C}, of 2 ms (typical of the rubbery amorphous phases of polymers), for the interphase material T_{2C} is $\sim$0.40 ms[1]. It should be noted that the mass fractions determined by both of the n.m.r. techniques are in good agreement.

Figure 5 shows the DD/MAS ^{13}C n.m.r. spectra of samples of Fraction 1, Rigidex 9, H020-54P, and Hifax. These spectra were obtained by the pulse sequence $[(\pi/4\text{–FID})_{HDD}\text{–}\tau_1]$ with a sufficiently long τ_1, without using the cross-polarization (CP) between ^{1}H and ^{13}C. Here, the waiting time τ_1 before each pulse was chosen to be longer than three times the longest spin-lattice relaxation time T_1 associated with the crystalline phase of each sample, as given for each spectrum. The CP technique was not used here, since the CP efficiency may be different according to the molecular motion of each individual component. Therefore, the spectra shown here reproduce exactly the contributions from all components in the samples, so giving us their mass fractions by component analysis, provided we know the elementary lineshape of each phase (as described below).

For all samples, there are distinctly recognizable sharp peaks assignable to the orthorhombic crystalline phase at $\sim$33 ppm from TMS. For samples H020-54P and Hifax, a monoclinic crystalline contribution is further recognized downfield at $\sim$34.4 ppm, in addition to the noncrystalline contribution at $\sim$31 ppm. For other samples, the existence of the noncrystalline contribution at 31 ppm is a little vague due to the high crystallinity, but the existence was clearly confirmed by enhancing the noncrystalline contribution using a shorter τ_1.

Spin-lattice relaxation (longitudinal relaxation). In order to examine the content of the crystalline contribution at 33.0 and 34.4 ppm and the noncrystalline

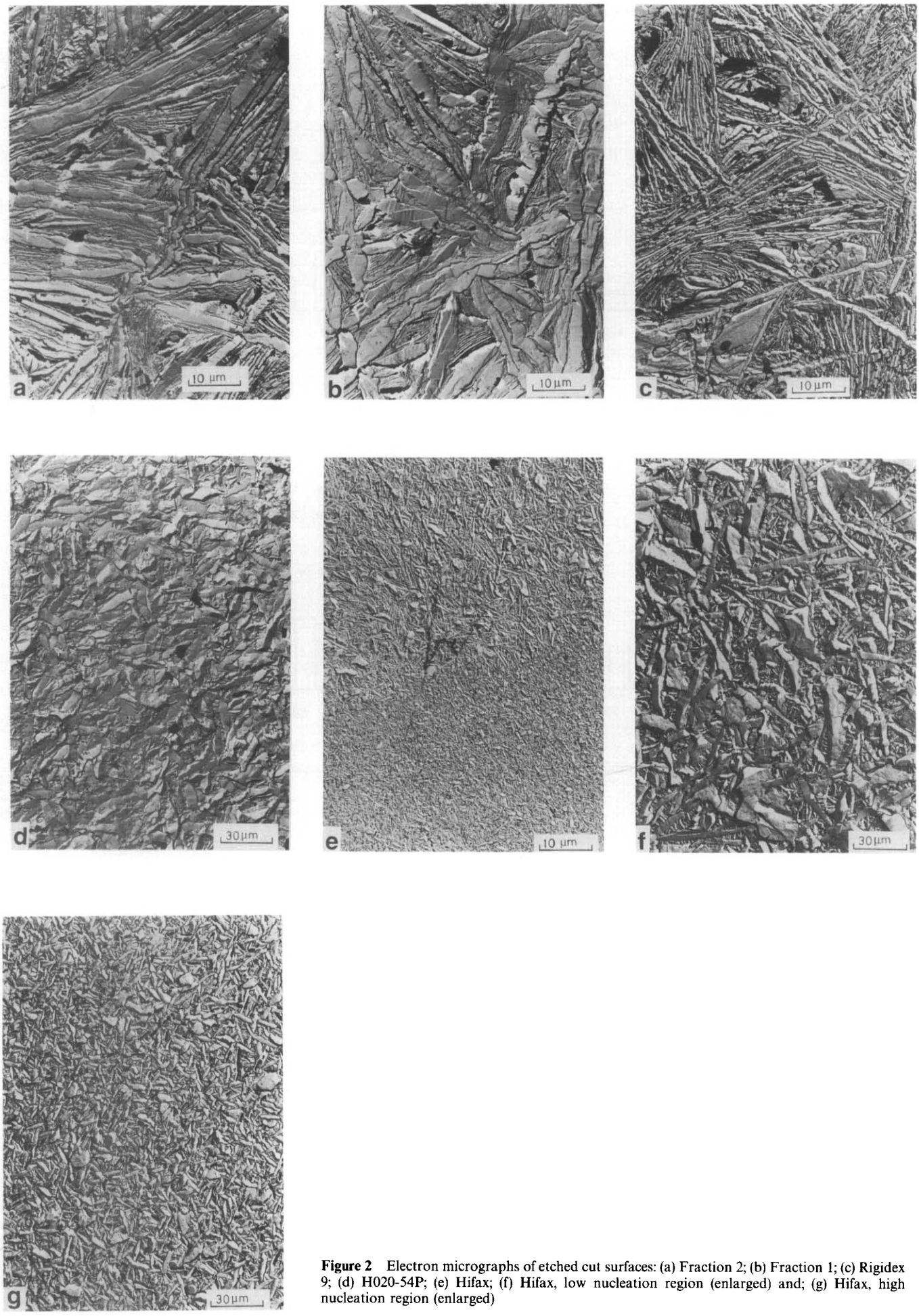

Figure 2 Electron micrographs of etched cut surfaces: (a) Fraction 2; (b) Fraction 1; (c) Rigidex 9; (d) H020-54P; (e) Hifax; (f) Hifax, low nucleation region (enlarged) and; (g) Hifax, high nucleation region (enlarged)

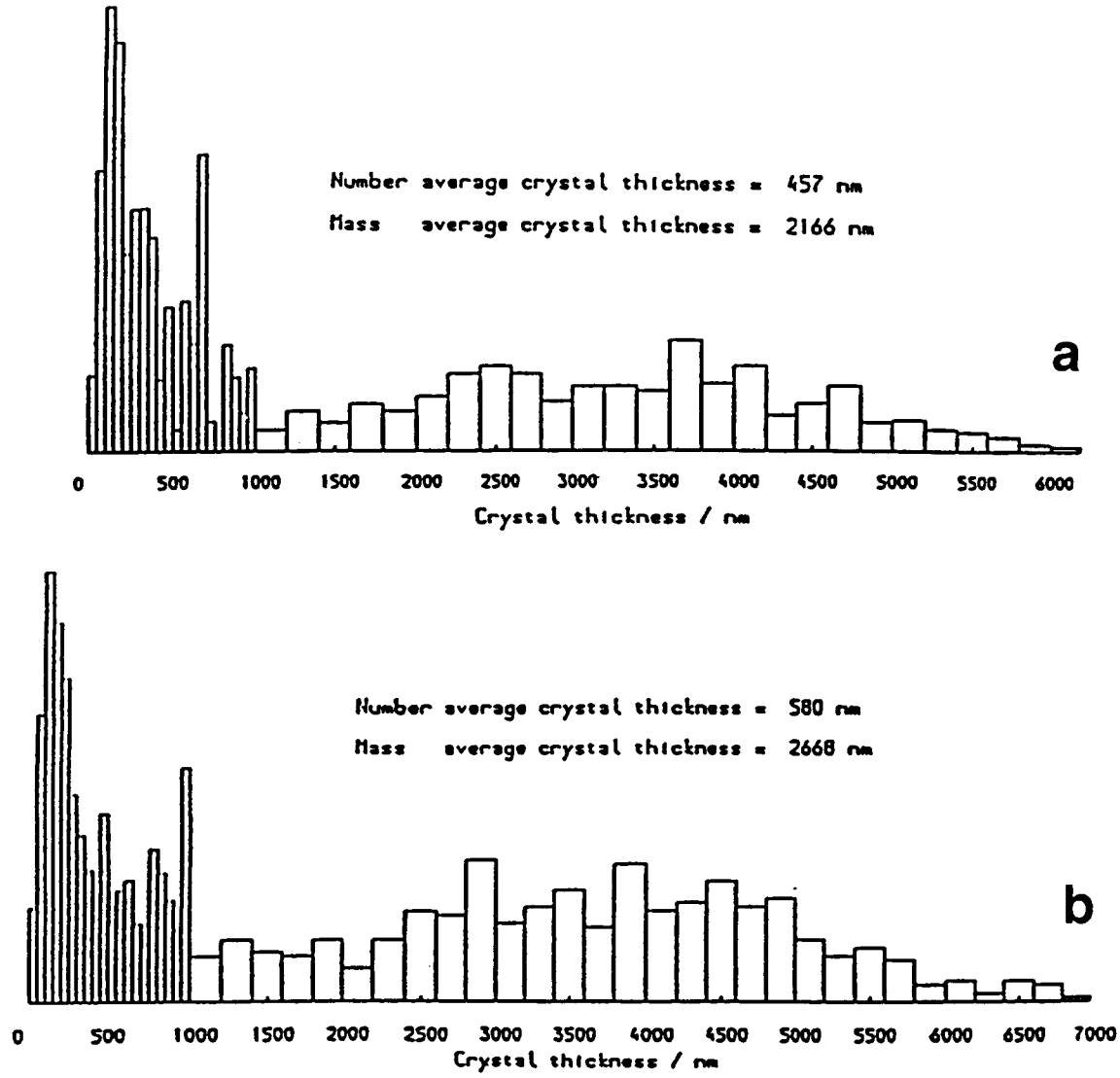

Figure 3 Distributions of lamellar thicknesses of Fraction 2 (a) and Fraction 1 (b) obtained by analyses of electron micrographs of fracture surfaces

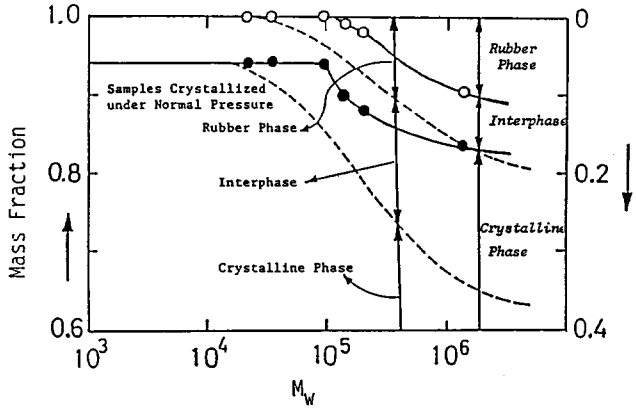

Figure 4 Mass fractions of three components of polyethylenes *versus* weight-average molecular weight, obtained from ^{1}H broad-line n.m.r. analyses. Solid lines indicate high-pressure-crystallized samples, while broken lines show samples which have been isothermally crystallized under atmospheric pressure

contribution at 31 ppm, the ^{13}C spin-lattice relaxation was observed. The T_{1C}s were generally measured by using Torchia's pulse sequence[10], but T_{1C}s shorter than 1 s were measured by a saturation-recovery method, modified for solid samples. The results are shown in *Table 3*. In this table, the ^{13}C spin-spin relaxation times T_{2C} are also presented; these will be discussed further later.

These data give a good indication of the characteristics of the phase structure of each sample. It is first noted that the T_{1C}s of the noncrystalline peak at ~31 ppm are in the range 0.35–0.50 s, without showing any appreciable differences among all of the samples. This is the same range as was previously reported[1] for all of the non-crystalline components in polyethylene which had been melt- or solution-crystallized at atmospheric pressure. T_{1C} is mainly determined by the frequency component, in the range of $\sim 10^8$ Hz, of the correlation function of the time-dependent dipole–dipole interaction due to the molecular motion. While these results suggest that the molecular motion of the noncrystalline phases in such a high-frequency motion associated with a local molecular chain motion is almost the same in all of the cases studied, it will be shown by consideration of T_{2C} that these noncrystalline phases are not equivalent in their molecular motion in a lower frequency range ($\sim 10^6$ Hz), whether one is comparing different phases in material crystallized either at atmospheric pressure[1] or high pressure.

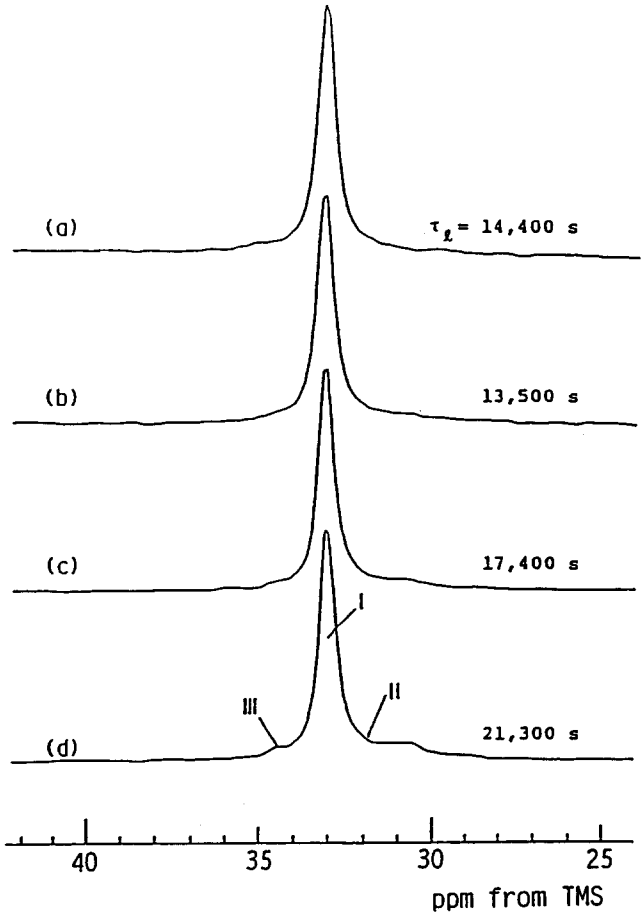

Figure 5 DD/MAS ^{13}C n.m.r. spectra of different polyethylene samples crystallized under high pressure, obtained by a $\pi/4$ single-pulse sequence $[(\pi/4)$–FID–$\tau_l]$: (a) Fraction 1; (b) Rigidex 9; (c) H020-54P and; (d) Hifax

Table 3 ^{13}C Spin-lattice and spin-spin relaxation times of high-pressure-crystallized polyethylene

	T_{1C}(s)		T_{2C}(ms)	
Sample	Crystalline (33 ppm)	Noncrystalline (31 ppm)	Interfacial	Amorphous
Fraction 2	4510, 526, 12	0.45	0.049	–[a]
Fraction 1	4720, 683, 11	0.50	0.050	–[a]
Rigidex 9	4320, 686, 46, 2	0.45	0.061	0.86
H020-54P	5710, 656, 21	0.40	0.010	2.2
Hifax 1900	7010, 810, 20, 2	0.35	0.020	2.0

[a] Not observed

On the other hand, the crystalline peak at 33 ppm does not exhibit a simple exponential longitudinal decay of ^{13}C magnetization and involves multiple (i.e. 3 or 4) T_{1C}s, as also reported for samples crystallized at atmospheric pressure, either from the melt or dilute solution[1]. Although the origin of the shortest two T_{1C}s has not yet been elucidated, the longest T_{1C} is assignable to the major part of the crystalline component that comprises lamellae with typical thicknesses.

Let us compare, first of all, the longest T_{1C} of each sample. In *Figure 6*, the longest T_{1C} of each sample is plotted against the number-average crystal thickness L_{Cn} given in *Table 1*. The data obtained for samples crystallized isothermally at atmospheric pressure, either from the melt[1] or dilute solution[3], and an uniaxially oriented sample[11], as well as the data reported by Axelson *et al.*[12], are also plotted for comparison. Axelson *et al.*[12] reported that the T_{1C} increases with increasing lamellar thickness for a wide variety of samples which differ in molecular character as well as in their crystallization conditions.

For our pressure-crystallized samples the T_{1C} generally increases with increasing crystal thickness, with the exception of Fractions 1 and 2. The T_{1C}s of samples H020-54P and Hifax are extremely long, i.e. 5710 and 7010 s, respectively, values which are much larger than those previously reported for this polymer[1,11,12]. However, these values are still shorter than those that might be expected from their extraordinarily large thicknesses. This can be explained on the basis of defects within the crystalline lamellae. The spin-lattice relaxation of a crystalline region without defects is thought to occur due to ^{13}C spin diffusion to the noncrystalline region with a shorter T_{1C}, and thus gives the L_{Cn} dependence of T_{1C}. Nevertheless, the spin-lattice relaxation may take place at the crystal defects if they are associated with a molecular motion. As a result, the T_{1C} loses its dependence on crystal thickness. As noted above, Fractions 1 and 2 include many molecular end groups within the crystalline lamellae. The fact that the T_{1C}s of these samples are appreciably shorter than the values expected from the largest crystal thicknesses is also in accord with relaxation taking place at defects.

Spin-spin relaxation (transverse relaxation). As pointed out in the last section, the noncrystalline component which contributes to the absorption at ~31 ppm comprises only one phase when judged by its T_{1C}, independent of the molecular character or the mode of crystallization of the samples. We have further examined the content of the 31 ppm line by the ^{13}C spin-spin relaxation which can detect molecular motion over a somewhat lower frequency range than the T_{1C}. For this purpose, we measured T_{2C} using the pulse sequence $[90°–\tau_t–(FID)_{DD}–\tau_l]$, i.e. the ^{13}C magnetization was turned 90° to the xy-plane (the

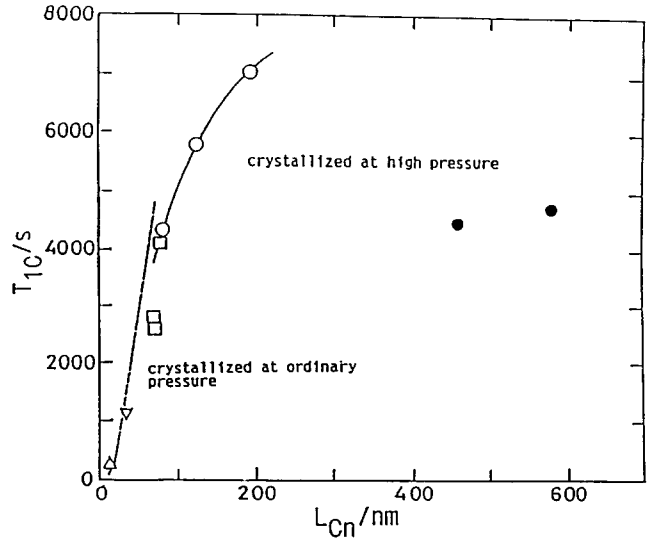

Figure 6 T_{1C} *versus* number-averaged crystal thickness, L_{Cn}, of various polyethylene samples: (○, ●) crystallized at high pressure, this work; (□) crystallized from the melt at ordinary pressure[1]; (▽) uniaxially drawn sample[11]; (△) single crystals from solution[3] and; (– – –) crystallized from the melt at ordinary pressure[12]

z-axis is parallel to B_0), and after being relaxed transversely for a chosen time the remaining ^{13}C magnetization was observed under ^1H decoupled conditions. For this measurement, we adopted a waiting time, τ_l, of 10 s. Since this τ_l was much shorter than the longer crystalline T_{1C}s of all of the samples, we could mainly identify the content of the noncrystalline component, in view of the decreased crystalline contribution.

As an example, the peak intensity at 31 ppm of Hifax is plotted against the relaxation time τ_t in *Figure 7*. In this figure, the upper open circles indicate the original data. It is evident that the decay curve consists of two steps, namely a rapid decrease in the initial step, which is followed by a slow decrease. The slow relaxation shows an exponential decay, as indicated by the continuous straight line, which gives T_{2C} to be 2.02 ms. Furthermore, if we replot the data in the initial step by subtracting the straight line, we obtain another straight line with the slope of $T_{2C}=0.020$ ms, as shown in the lower part of the figure. Hence, it is evident that, although the noncrystalline component of this sample is regarded as consisting of only one phase by virtue of the spin-lattice relaxation time T_{1C}, it consists of two phases when examined from the point of view of T_{1C}.

This fact will be more clearly recognized by looking at the actual line shapes at each relaxation step. *Figure 8* shows the actual spectra at each transverse relaxation step, corresponding to the relaxation data in *Figure 7*. Because of the shorter waiting time ($\tau_l=10$ ms) adopted, in comparison to the crystalline T_{1C}s, these spectra represent mainly the transverse relaxation of the noncrystalline component. At the starting point of the relaxation, i.e. at $\tau_t=0.5\,\mu$s, one observes the total contribution from all of the noncrystalline components with a minor remaining contribution from the crystalline component at 33 ppm. However, as the relaxation proceeds, this crystalline contribution rapidly disappears, and only the noncrystalline contribution at 31 ppm remains. At $\tau_t>100\,\mu$s, the spectrum becomes Lorentzian with a linewidth of ~ 1.1 ppm. From this, the spectrum at $\tau_t>100\,\mu$s, which is five times longer than T_{2C} at the initial stage in the figure, is assignable to an amorphous phase with a random molecular chain conformation and

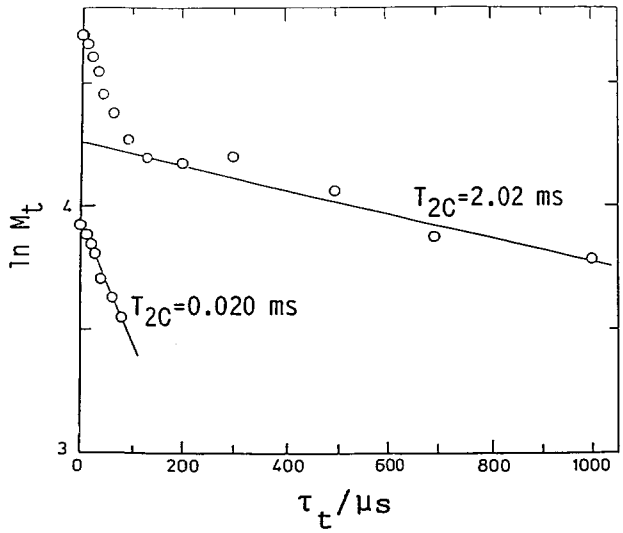

Figure 7 ^{13}C spin-spin relaxation behaviour of the noncrystalline component of Hifax

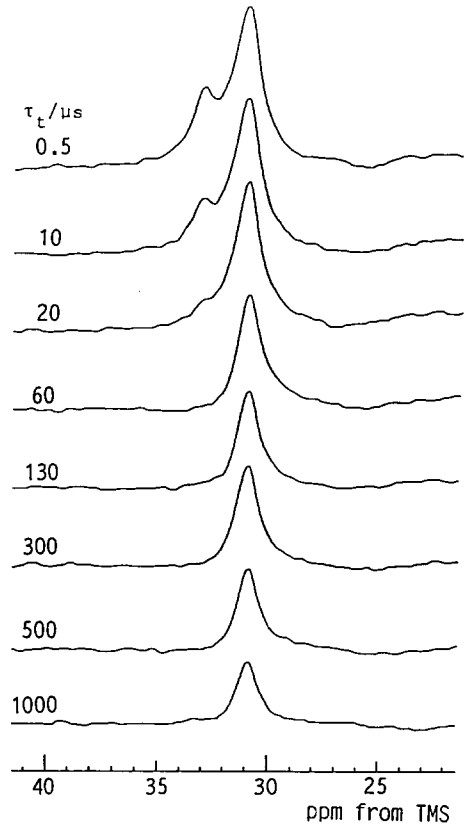

Figure 8 Partially relaxed spectra of the noncrystalline component of Hifax, measured by the pulse sequence $[(\pi/2)$–τ_t–FID–$\tau_l]$ with $\tau_l=10$ ms

rubbery molecular motion. On the other hand, the lineshape of the noncrystalline component with a T_{2C} of 0.02 ms is obtainable from the partially relaxed spectrum at $\tau_t=0.5\,\mu$s by subtracting the contributions from the crystalline and the rubbery-amorphous noncrystalline components. Due to its broad lineshape and its very short T_{2C}, this other noncrystalline component is assignable to a phase with a restricted molecular confirmation and molecular motion.

Some of the present authors[1] have previously found two noncrystalline phases, with a common T_{1C}, but with different T_{2C}s, in a similar way for bulk crystals crystallized at atmospheric pressure, where the long and short T_{2C} components were assigned, respectively, to an amorphous phase and a crytalline–amorphous interphase. Since the T_{2C}s obtained here for Hifax are almost the same as those of the bulk crystals crystallized at atmospheric pressure, it is assumed that the phase structure of the Hifax is essentially the same, consisting of three phases, i.e. a very stable crystalline phase composed of lamellae with very large thicknesses, a crystalline–amorphous interphase, and an amorphous phase. Similar data that suggest two different noncrystalline phases were obtained for sample H020-54P.

The situation is somewhat different for the lower-molecular-weight materials, Fractions 1 and 2. The data obtained for Fraction 2 are displayed in *Figures 9* and *10*. The change of the peak intensity at 31 ppm according to the transverse relaxation is shown in *Figure 9* and the actual relaxed spectra at each relaxation time τ_t are shown in *Figure 10*. The two-step transverse relaxation, as recognized for Hifax, is not seen in this case and the logarithm of the magnetization decreases linearly with τ_t, giving a T_{2C} of 49 μs, so that only one kind of

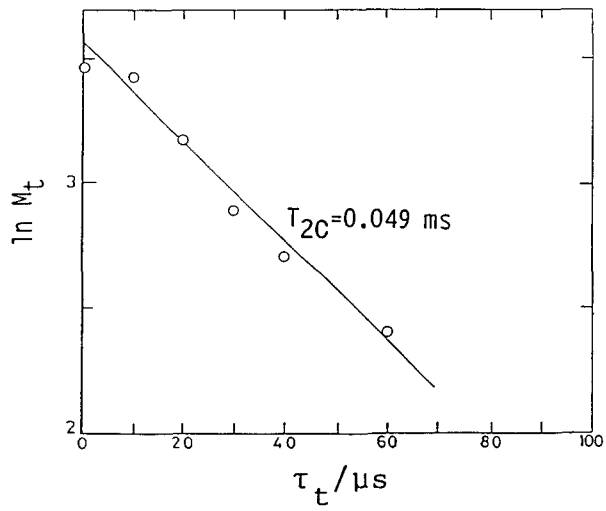

Figure 9 ^{13}C spin-spin relaxation behaviour of the noncrystalline component of Fraction 2

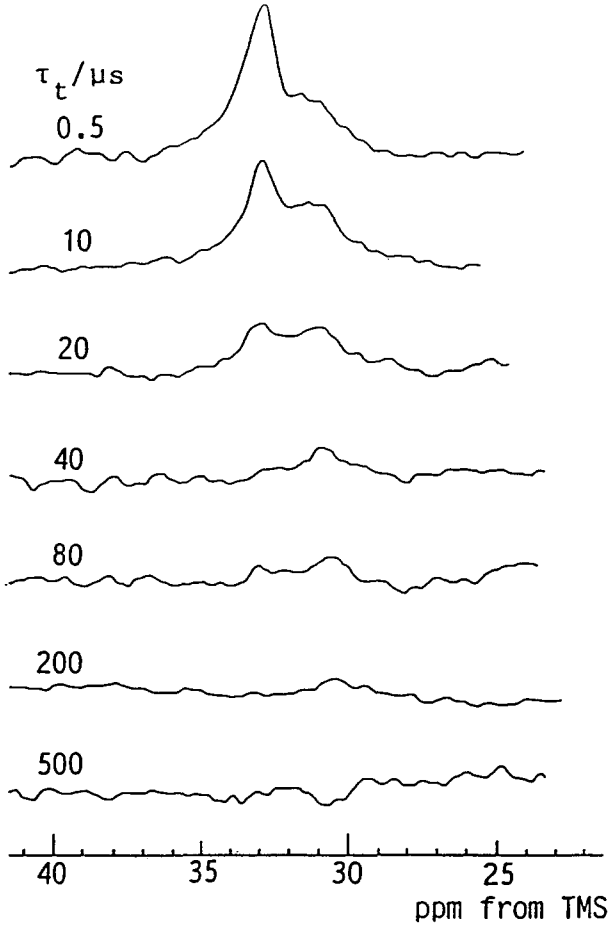

Figure 10 Partially relaxed spectra of Fraction 2, measured by the pulse sequence $[(\pi/2)$–τ_t–FID–$\tau_l]$ with $\tau_l = 10$ s

noncrystalline component is evident. This can be confirmed by the data presented in *Figure 10* where the spectrum has actually disappeared by $\tau_t > 200\,\mu$s, without showing any contribution from the rubbery component (as recognized for Hifax). Similar results were obtained for Fraction 1. It is thus concluded that these samples comprise lamellar crystallites and a noncrystalline overlayer, and is devoid of the rubbery-amorphous component. This is in agreement with the conclusion reached by the ^1H broad-line n.m.r. analysis that those samples with a molecular weight which is lower than 10^5 are devoid of any rubbery component. In Rigidex 9, the rubbery amorphous phase only appears to a level of ~1%, and is not associated with pronounced molecular mobility, as found with the higher-molecular-weight samples. This is in keeping with its much shorter T_{2C} of 0.86 ms.

The T_{2C} values of all of the samples are listed in *Table 3*, along with the corresponding T_{1C}s. These data characterize definitely the phase structure of each sample in terms of chemical shift and relaxation times.

Line-shape analyses, mass fraction and thickness of each phase. As already discussed, the DD/MAS ^{13}C n.m.r. spectra shown in *Figure 5* represent, exactly, the contributions from all components of the samples, i.e. the crystalline and two noncrystalline phases, as a result of the longer waiting time τ_l that is used. It is possible to decompose these spectra into three components, provided the elementary lineshapes of all components are known. First of all, it was confirmed that the crystalline absorptions representing the contributions from the crystalline phases in both the orthorhombic and monoclinic forms could be well reproduced by two Lorentzians with a linewidth of ~0.6 ppm, centred at 33.0 and 34.4 ppm, respectively, although the former line was associated with multiple T_{1C}s. To obtain the elementary line shape of the amorphous rubbery phase, the partially transverse relaxed spectra, after the disappearance of all contributions from other phases, can be used. For Hifax, for example, the spectrum A at $\tau_l = 10$ s and $\tau_t = 0.5\,\mu$s, shown in *Figure 11* comprises full contributions from

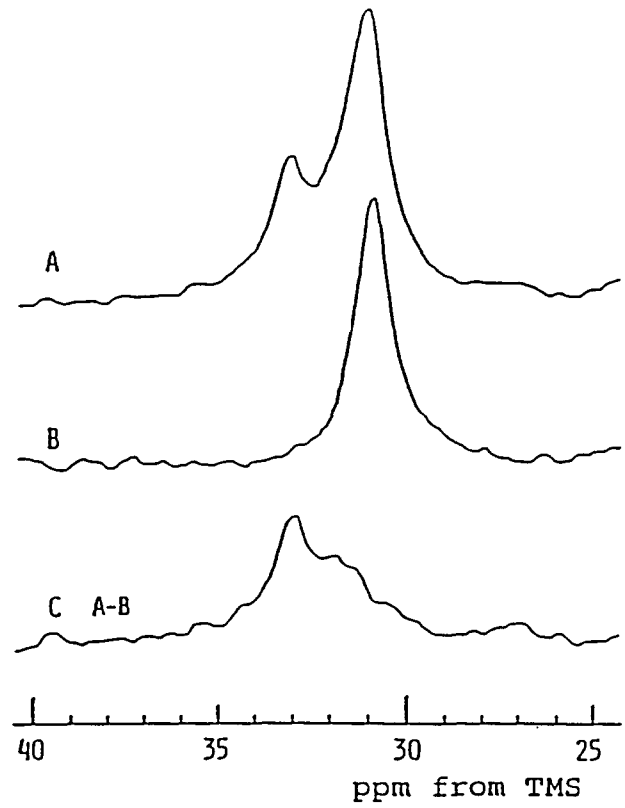

Figure 11 Component spectra of Hifax: (A) obtained by the pulse sequence $[(\pi/2)$–τ_t–FID–$\tau_l]$ with $\tau_l = 10$ s and $\tau_t = 0.5\,\mu$s; (B) obtained by the same pulse sequence as for A, with $\tau_l = 10$ s and $\tau_t = 130\,\mu$s and; (C) difference spectrum (A–B) (spectra A and B were taken from *Figure 8*)

the crystalline–amorphous interphase and the rubbery amorphous phase, with a minor contribution from the crystalline phases, while spectrum B ($\tau_l = 10$ s and $\tau_t = 130\,\mu$s) shown in this figure contains only the contribution from the rubbery amorphous phase, and can be approximated to be a Lorentzian with a linewidth of ~1.1 ppm centred at ~31.0 ppm. Therefore, by subtracting the Lorentzian obtained from spectrum B from spectrum A, one obtains the difference spectrum C, consisting of the elementary line shape for the crystalline–amorphous interphase and a minor contribution from the crystalline phases. This can be further decomposed into two components, namely a Lorentzian at 33 ppm with a linewidth of ~1 ppm as the crystalline contribution, and a somewhat broad symmetric line with a linewidth of ~2.5 ppm, which can be used as the elementary line shape for the crystalline–amorphous interphase.

Using these elementary line shapes for all of the components, a line-shape analysis was carried out for the DD/MAS ^{13}C n.m.r. spectrum of Hifax. The result is shown in *Figure 12*, together with the integrated intensity fractions of the respective components. It is seen that the composite curve indicated by a broken line reproduces well the observed spectrum. A similar line-shape analysis was also carried out for H020-54P but could not be achieved with sufficient precision for Fractions 1 and 2, or for Rigidex 9, because of their high crystallinities.

If we assume the typical lamellar structure for these samples, the thickness of each phase can be estimated by using the mass fraction values obtained from the line-shape analysis and the crystalline stem lengths measured by other techniques. The thicknesses of the crystalline–amorphous interphase and the amorphous phase, L_i and L_a, respectively, may be estimated by:

$$L_i = L_c f_i / 2(f_{c1} + f_{c2}) \quad (1)$$

$$L_a = L_c f_a / (f_{c1} + f_{c2}) \quad (2)$$

where L_c is the crystalline stem length or the lamellar thickness, and f_{c1}, f_{c2}, f_i and f_a denote, respectively, the volume fractions of the crystalline (orthorhombic and monoclinic), the crystalline–amorphous and the amorphous components. Since values of the crystalline stem length or the lamellar thickness involve a wide distribution and also depend on the method of estimation, the situation is not so simple. Here, however, the weight-average crystal thickness, estimated from the nitric acid degradation/g.p.c. technique, was used[14]. The results are shown in *Table 4*, together with the mass fraction values of each phase, as derived from the line-shape analysis.

It is seen that for both samples the crystalline mass fraction (orthorhombic plus monoclinic) agrees well with that estimated by the density measurements and ^1H broad-line n.m.r. analysis. It is seen that the thicknesses of the interphases are 3.8 and 8.0 nm for H020-54P and Hifax, respectively. The value obtained for H020-54P is almost the same as the 3.4 nm reported for the atmospheric-pressure-crystallized samples with normal molecular weights in the range 30 000–150 000[1]. On the other hand, the value for Hifax is significantly larger than the reported values for other types of sample, as well as the values of 1.5–2.0 nm which were evaluated theoretically by Flory *et al.*[13]. The increase in the thickness of the interfacial phase was also noted for the atmospheric-pressure-crystallized samples if the molecular weight exceeds 150 000.

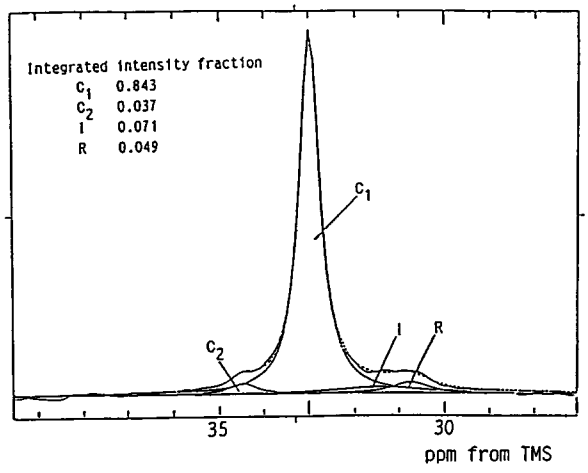

Figure 12 Component analysis of the fully relaxed ^{13}C n.m.r. spectrum of Hifax: C_1 = orthorhombic crystalline; C_2 = monoclinic crystalline; I = interfacial and; R = rubbery

Phase structure of samples

As can be seen in *Figure 4*, the dependence of the phase structure on molecular weight shifts to the higher-molecular-weight side in comparison with samples crystallized at atmospheric pressure, and in particular, the rubbery-amorphous component appears above a molecular weight of 30 000 for atmospheric-pressure-crystallized samples, but above a value of 100 000 for samples crystallized at high pressure. The significance of this appears to lie in the polydispersity of the relevant samples. The previously studied atmospheric-pressure-crystallized samples[3] were fractions with a molecular-weight polydispersity of ~2, so at $\bar{M}_w = 30\,000$ the *number*-averaged extended molecular chain length X_n is

Table 4 Mass fractions and thicknesses of crystalline and noncrystalline phases

	Mass fraction				Thickness of each phase[a] (nm)		
	Crystalline		Noncrystalline				
Sample	Orthorombic	Monoclinic	Interfacial	Amorphous	Crystalline	Interfacial	Amorphous
H020-54	0.874	0.017	0.055	0.053	120	3.8	7.3
Hifax	0.843	0.037	0.071	0.049	90	8.0	11.0

[a] Estimated from the crystalline stem lengths (or lamellar thicknesses) and mass fractions of the phases by using equations (1) and (2) where the volume fraction of all phases was assumed to be equal to the mass fraction, i.e. the densities of all phases were assumed to be unity in these estimations. This assumption may not introduce any appreciable influence on other aspects of the discussion of this work

approximately twice the number-averaged crystal thickness L_n. Below the limit of 2 for the ratio X_n/L_n, a molecular chain participates only once in a crystallite and the so-called extended crystals are produced; the noncrystalline molecular chains consist of the crystallite overlayer. If the ratio X_n/L_n exceeds 2, a molecular chain comes to participate repeatedly in a crystallite by chain folding and the amorphous phase is thought to appear. On the other hand, with regard to the pressure-crystallized samples, the rubbery-amorphous phase could only just be detected by the ^1H broad-line analysis even for the Rigidex 9 sample with $\bar{M}_w = 132\,000$. The fit here does not at first sight appear so good, since the number-averaged chain length (115 nm) is little bigger than the number-averaged crystal thickness (82 nm). However, during high-pressure crystallization considerable molecular fractionation into discrete crystal populations occurs, and taking this into account there is good reason to suppose that the same presence or absence of repeat folding is the determining factor. For the samples with higher molecular weights that involve the rubbery amorphous component, X_n/L_n and X_w/L_w are ~ 2.2 and 7.5–26, respectively. It is then reasonable, even in the pressure-crystallized samples, that a molecular chain participates repeatedly in a crystallite or several crystallites by chain folding and the amorphous phase appears.

CONCLUSIONS

A study by n.m.r. spectroscopy combined with morphological techniques, including electron microscopy, has shown how it is possible to obtain a more thorough determination of the distribution of the phase structure in various polyethylene samples crystallized at high pressure based on both ^1H broad-line and ^{13}C n.m.r. spectroscopic analyses. Three phases, namely a lamellar crystalline, a crystalline–amorphous interphase and an amorphous phase occur in polymers of high molecular weight but the amorphous phase is absent from lower-molecular-weight materials. It is inferred that the rubbery amorphous phase appears in both atmospheric and high-pressure-crystallized samples, when the number-averaged molecular chain length exceeds double the number-averaged crystal thickness, allowing repetitive chain folding. In general, the phase structures obtained by the combined n.m.r. techniques, including details of the defects in the crystalline lamellae, are consistent with the deductions of the morphological analysis obtained by g.p.c. and electron microscopy.

REFERENCES

1 Kitamaru, R., Horii, F. and Murayama, K. *Macromolecules* 1986, **19**, 636
2 Jackson, J. B., Flory, P. J. and Chiang, R. *Trans. Faraday Soc.* 1963, **59**, 1906
3 Kitamaru, R. and Horii, F. *Adv. Polym. Sci.* 1978, **26**, 137
4 Kitamaru, R., Horii, F. and Hyon, S.-H. *J. Polym. Sci., Polym. Phys. Edn* 1977, **15**, 821
5 Olley, R. H. and Bassett, D. C. *J. Polym. Sci., Polym. Phys. Edn* 1977, **15**, 1011
6 Olley, R. H., Hodge, A. M. and Bassett, D. C. *J. Polym. Sci., Polym. Phys. Edn* 1979, **17**, 672
7 Rees, D. V. and Bassett, D. C. *Polym. Lett.* 1969, **7**, 273
8 Bassett, D. C. and Turner, B. *Philos. Mag.* 1974, **29**, 285
9 Bassett, D. C., Hodge, A. M. and Olley, R. H. *Proc. R. Soc. London A* 1981, **377**, 39
10 Torchia, D. A. *J. Magn. Reson.* 1978, **30**, 631
11 Nakagawa, M., Horii, F. and Kitamaru, R. *Polymer* 1990, **31**, 323
12 Axelson, D. E., Mandelkern, L., Popli, R. and Mathieu, P. *J. Polym. Sci., Polym. Phys. Edn* 1983, **21**, 2319
13 Bassett, D. C., Khalifa, B. A. and Olley, R. H. *J. Polym. Sci., Polym. Phys. Edn* 1977, **15**, 995
14 Flory, P. J., Yoon, D. Y. and Dill, K. A. *Macromolecules* 1984, **17**, 862, 868